The Journal of Chemical Physics ARTICLE scitation.org/journal/jcp

Generative adversarial networks for transition state geometry prediction

Cite as: J. Chem. Phys. 155, 024116 (2021); doi: 10.1063/5.0055094
Submitted: 25 April 2021 • Accepted: 28 June 2021 •
Published Online: 13 July 2021

Małgorzata Z. Makoś,[1] Niraj Verma,[1] Eric C. Larson,[2] Marek Freindorf,[1] and Elfi Kraka[1,a)]

AFFILIATIONS

[1] Computational and Theoretical Chemistry Group (CATCO), Department of Chemistry, Southern Methodist University, 3215 Daniel Avenue, Dallas, Texas 75275-0314, USA
[2] Computer Science Department, Southern Methodist University, 3215 Daniel Avenue, Dallas, Texas 75275-0314, USA

[a)] **Author to whom correspondence should be addressed:** ekraka@gmail.com

ABSTRACT

This work introduces a novel application of generative adversarial networks (GANs) for the prediction of starting geometries in transition state (TS) searches based on the geometries of reactants and products. The multi-dimensional potential energy space of a chemical reaction often complicates the location of a starting TS geometry, leading to the correct TS combining reactants and products in question. The proposed TS-GAN efficiently maps the space between reactants and products and generates reliable TS guess geometries, and it can be easily combined with any quantum chemical software package performing geometry optimizations. The TS-GAN was trained and applied to generate TS guess structures for typical chemical reactions, such as hydrogen migration, isomerization, and transition metal-catalyzed reactions. The performance of the TS-GAN was directly compared to that of classical approaches, proving its high accuracy and efficiency. The current TS-GAN can be extended to any dataset that contains sufficient chemical reactions for training. The software is freely available for training, experimentation, and prediction at https://github.com/ekraka/TS-GAN.

I. INTRODUCTION

Generative models have been historically applied in statistical machine learning (ML) and have shown great potential in image processing, computer vision, natural language processing, and the medical field.[1–3] Generative models are required to know as much as possible about the data, as generating one is in itself a complex process. A remarkable generative model first introduced by Goodfellow *et al.*[4] and termed Generative Adversarial Network (GAN) has gained significant attention. In this approach, neural networks automatically learn and discover patterns and regularities in the input data that are necessary to generate new examples that plausibly could have been drawn from the original dataset.[4]

Originally, GANs were designed to generate realistic synthetic images from a random distribution vector. Isola *et al.*[5] realized that a slight modification of the GAN by including a condition to have a one-to-one mapping between a pair of input and output resulted in the generation of realistic outputs from a given input. Conditional GANs have been demonstrated as a general-purpose solution for image-to-image translation tasks, e.g., converting black and white photographs to color, maps to satellite photographs, and sketches of products to product photographs.[5]

In this work, we explored the possibility of utilizing a conditional GAN to predict a transition state (TS) guess geometry of a chemical reaction by mapping the space between reactants and products to that of the TS. TS searches are common operations for kinetic modeling (e.g., variational transition state theory[6]) and studying the mechanism of chemical reactions. However, finding TSs is a challenge in itself, especially if the reaction is complex, and different reaction paths may occur.[7,8] Often, the calculation of TS structures strongly depends on the topology of the underlying potential energy surface (PES),[9,10] the sophistication of the search algorithm, as well as additional inputs such as information about the stoichiometry of the TS from kinetic data or details about the atoms involved in the bond-forming/breaking processes.[11,12] A necessary prerequisite for finding the TS is a good TS guess geometry to start from, which is typically constructed manually and adjusted accordingly in a trial-and-error fashion based on chemical intuitions, such as Hammond's postulate.[13] As a result, chemical knowledge and manual intervention are essential, yet this

does not necessarily lead to the optimal mathematical solution. Popular TS search methods incorporated in most common quantum chemistry packages are the Berny algorithm,[14] synchronous transit-guided quasi-Newton (STQN) method,[15] minimum energy path procedures,[16] Newton–Raphson type method procedures using approximate Hessians,[17] and Hessian update schemes,[18–22] just to name a few. Although Hessian involved methods should be most effective,[23] depending on the TS guess, the Hessian matrix may not have the appropriate number of negative eigenvalues (i.e., just one for a chemically meaningful TS of first order) requiring further correction, e.g., a rational function technique;[24] they are also computationally expensive, in particular, for larger reaction systems.

Over the years, several methods to generate approximate TS structures were proposed. For instance, the growing string method uses driving coordinates from reactants to find products from which the TS can be generated,[25] TS prediction within the Reaction Mechanism Generator (RMG) framework,[26,27] the AARON code[28,29] that automatically generates initial TS structures based on a library of TS templates, and AutoTST[30,31] that automates TS searches for high-throughput computational kinetics; in addition, approaches that explore the PES have been reported.[32–36]

Recently, ML-based models have made remarkable progress in chemistry,[37–43] including TS search approaches.[44–46] For instance, approaches based on Gaussian process regression were reported to improve classical Hessian update methods,[47,48] find minimum energy paths,[23] and predict activation energies.[49] Kernel ridge regression methods were also applied to construct ML potentials, from which the TS was found.[50] Pattanaik *et al.*[51] presented a method for predicting TS for isomerization reactions using a graph neural network, showing a 71% accuracy, mainly failing for large structures and reactions with symmetric TSs. Overall, these methods have been proven to be attractive new tools in TS searches significantly reducing the computational expenses; however, current methods are mostly subject to limitations caused by the complexity of the code or the amount of required input, and they tend to favor one type of reaction.[28,29,31,51]

This work presents a novel approach to generate TS guess geometries based on a conditional GAN using the Cartesian coordinates of the reactant and product as only input, avoiding expensive mapping of reaction paths or PES regions. The underlying goal was to design a method that is simple to use, does not favor any reaction type or size of the reaction complex, and can be easily expanded. The applicability of our new TS-GAN was assessed for various chemical reactions, including hydrogen transfer/migration reactions, isomerization reactions, and multi-step reactions involving transition metal catalysts.

II. METHODS

In the following, we first describe the datasets utilized in this work to train the TS-GAN model. The data consist of Cartesian coordinates of each atom of reactant, product, and TS pairs, which were converted to features, discussed in Sec. II B. The features are directly utilized by the TS-GAN model, the architecture of which is discussed in detail below. The TS-GAN model converts the features back to predict the coordinates of each atom for the TS guess geometry. The performance of the TS-GAN model was compared with that of other classical approaches based on geometrical similarity and the ability to predict starting coordinates for the TS close to the final TS geometry.

A. Datasets

We trained our model on three separate datasets; each contains optimized Cartesian coordinates of reactants, TS, and products. Dataset **A** contains over 500 reactions, including hydrogen abstractions, intramolecular hydrogen migration, hydrogen transfer, and a hydrogen addition to multiple bond reaction families (here, referred to as H-migration reaction). The structures in **A** involve anywhere from 3 to 55 atoms, including H, C, N, and O. Many of the reactions are similar to those in RMG,[27] GMTKN55,[52] and Baker's[53] datasets, from where only the H-migration reactions were chosen to cover a wide range of the typical and less common chemical reactions. The coordinates of reactants, TS, and products of all set A reactions are included in the supplementary material.

We note that various density functional theory (DFT) methods including B3LYP, M06, and ωB97X levels of theory[54–57] in connection to def2-TZVP and 6-31G*(d,p) basis sets[54–56] were utilized to optimize the TS geometry for dataset **A**. Each of the transition states was validated using an intrinsic reaction coordinate (IRC) calculation[58] by the authors, and the reactant and product structures were calculated at the same level of theory as TS.

A recently published dataset by Grambow, Pattanaik, and Green[59] contains a total of 12 000 reactions generated with the single-ended growing string method involving anywhere from 4 to 21 atoms including H, C, N, and O. From this dataset, we choose ~9500 reactions that were optimized with ωB97X-D3/def2-TZVP level of theory, similarly to the recently published ML-based method for generating the TSs of isomerization reactions by Pattanaik *et al.*[51] as dataset **B**.

Dataset **C** contains only reactions including transition metals, where many of them are multi-step catalyzed reactions. The applicability of this dataset is not specific to any problem, but instead is designed to investigate the feasibility of our approach. Dataset **C** is based on Unified Reaction Valley Approach (URVA) studies of the CATCO group[60] at the Southern Methodist University, Dallas TX, USA. URVA is a popular tool to analyze the reaction mechanism of a chemical reaction via the analysis of the reaction path and the surrounding reaction valley on the potential energy surface.[60] For the purpose of our work, we selected geometries of reactants, TSs, and products of about 400 chemical reactions from previous URVA studies focusing on transition metals. Catalytic reactions in dataset **C** contain the following transition metals: Ti, Fe, Ni, Cu, Ru, Rh, Pd, Re, Ir, Pt, Au, and Hq. Table S1 of the supplementary material shows the original citations for selected reactions.

The TS-GAN method was trained separately for each dataset. Across all reaction complexes, datasets **A** and **B** were divided randomly into an 80:20 manner. In other words, geometries of reactants, TSs, and products of 80% of the reactions were used for training and 20% of the reactions for testing. For dataset **C**, 15 reactions based on Ru, Au, and Ni were kept as a test set.

B. Data representation

The molecular three-dimensional Cartesian coordinates were converted into the Coulomb matrix (CM). It is found to be an

excellent descriptor because of its complete analogy to the electronic Hamiltonian used in *ab initio* methods.[61] CM is frequently used, especially in the ML approaches for predicting atomization energies,[61,62] excitation energies,[63] electronic and charge transfer couplings,[64,65] and to study molecular materials.[64,66–68] CM was formulated as mentioned by Rupp *et al*,[61]

$$\mathbf{M_{ij}} = \begin{cases} 0.5Z_i^{2.4} & \forall \quad i = j, \\ \dfrac{Z_iZ_j}{|\mathbf{R}_i - \mathbf{R}_j|} & \forall \quad i \neq j, \end{cases} \tag{1}$$

where Z_i is the nuclear charge and R_i contains the nuclear coordinates of atom i as a vector. The coefficients in the diagonal elements are based on the polynomial fit of atomic energies to nuclear charge.[61]

Since CM is defined in terms of relative atomic coordinates, it is invariant under rotations and translations of the molecule. This gives the distance between atoms regardless of the choice of origin and makes it a unique descriptor as no two molecules will have the same CM unless they are identical. We find that the CM representation is sufficient for our purposes, efficiently calculated and easily interpretable, making it a natural choice. However, a number of other representations may also achieve good performance such as weighted graph neural networks.[69] We leave this investigation for future work.

The size of the CM depends on the number of atoms in the molecule. Because our dataset contains reaction complexes of different sizes, a constant dimensionality for the input is desired. Therefore, the fixed length of $\mathbf{M_{ij}}$ is set to 100. For molecules with the number of atoms less than 100, the $\mathbf{M_{ij}}$ is padded with zeros. Note that each of the dataset does not contain complexes with more than 100 atoms. CMs of all datasets are available on the GitHub page.[70]

C. Architecture of TS-GAN

A major problem faced by single architecture of neural networks such as Convolutional Neural Networks (CNNs) is the loss function. For example, a neural architecture that minimizes the Euclidean distance between two sets of images will result in the generation of blurry images due to the averaging of all distances.[71,72] In this work, we utilize GANs that add an adversarial network as a decoder to the generated image so that the loss is minimized in such a way that the "output is indistinguishable from reality."[5] The remarkable idea of adding an adversarial network was first shown by Goodfellow *et al.*,[4] where a generator G maps random noise vector z to the desired output y ($G : x \rightarrow y$). In our case, the condition is applied to consider input vector x with z to map y ($G : \{x, z\} \rightarrow y$). The objective of the conditional GAN is expressed by the loss function L,

$$L(G, D) = \mathbb{E}_{x,y}[\log D(x, y)] + \mathbb{E}_{x,y}[\log(1 - D(x, G(x, z)))], \tag{2}$$

where G minimizes the objective against discriminator D that tries to maximize it and $\mathbb{E}_{x,y}$ refers to the expected value,

$$G^* = \arg\min_G \max_D L(G, D). \tag{3}$$

The G network predicts the required output (CM of TS in our case), which is pitted against an adversary D network. The objective of the D network is to determine whether the output predicted from the G network is from model distribution (fake) or data distribution (real). As stated by Goodfellow *et al.*, the G network can be thought of as counterfeiters that produce fake currency and use it without detection, while the D network acts as police and detects counterfeit currency. The competition between G and D networks allows both to improve until the data distribution of fake and real is undistinguishable. In a similar fashion, Eq. (3) is applied where G must minimize the objective against discriminator D that tries to maximize the objective. We note that, technically, the GAN model can be trained without z; however, this would result in deterministic outputs and will fail to find patterns outside the delta function. The generator and discriminator architectures were adopted from Isola *et al.*,[5] such as convolutional network architecture, convolution-BatchNorm-ReLU, LeakyRELU for each convolution network output, and dropouts for several layers in the generator.

The CNNs can be thought of as filters that learn to multiply weights to extract crucial information from the data such as facial parts from a hypothetical CNN model that recognizes face. In this way, such models can learn local features from the data. Providing multiple CNNs enhances the learning of further intricate patterns from the data as shown through visualizing CNNs by Fu *et al.*[73] Thus, we utilize such an architecture for G motivated from Isola *et al.*, as shown in Fig. 1. In a similar fashion, D was composed of three CNNs. Since the prediction task of D is to predict a single value between 0 and 1, increasing the number of CNNs did not significantly improve the performance. The CMs of reactants and products (R and P) are provided as input x to the generator. As the output, the generator predicts synthetic TS z. In the next step, the fake pair (x, z) is created by concatenating the R and P input and the output of the generated model, while the R and P and the real TS form the real pair (x, y). The created pairs are concatenated into a tensor that is fed as the input to the discriminator network.

The generated CMs of the TS geometries are converted back into three-dimensional Cartesian coordinates. In order to do so, we developed an optimization process based on the distance matrix. The initial structure for a TS geometry was taken as the mean of reactant and product coordinates. We note that no significant difference in the final geometry was observed when initial coordinates were random set of numbers. Having the initial guess of TS coordinates,

$$\mathbf{C}_{init} = [C_1^0, C_2^0, \ldots, C_{3N}^0], \tag{4}$$

where N is the number of atoms, the transition state coordinates can be determined by iterating over $\mathbf{C}_{init}$,

$$\mathbf{C}_{ts} = \mathbf{C}_{init} + f(C), \tag{5}$$

where $f(C)$ is a function of C determined by following the loss l to a minimum. Given a CM, the distance matrix $\mathbf{D}$ is calculated by

$$\mathbf{D_{ij}} = \begin{cases} 0 & \forall \quad i = j, \\ \left(\dfrac{\mathbf{M_{ij}}}{Z_iZ_j}\right)^{-1} & \forall \quad i \neq j, \end{cases} \tag{6}$$

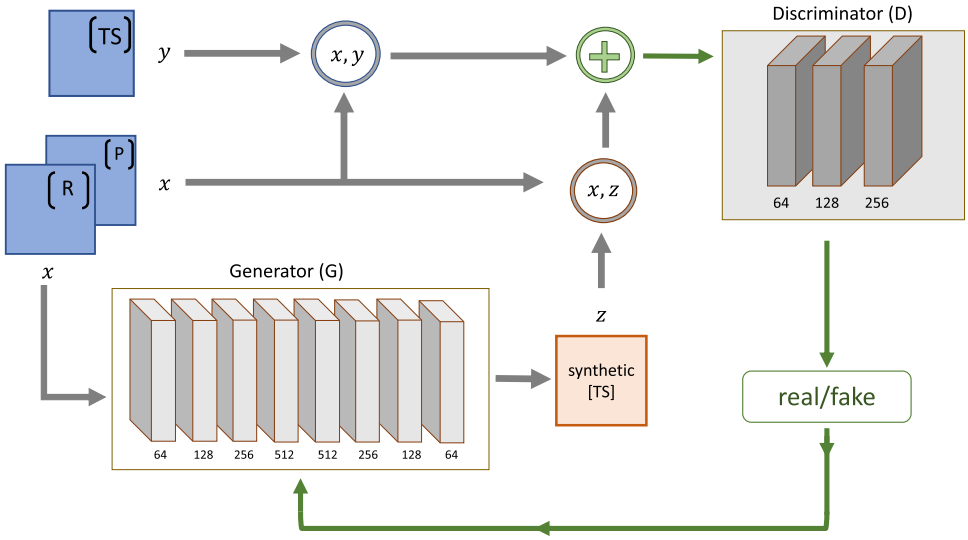

FIG. 1. Architecture of TS-GAN. The CMs extracted from the coordinates of reactants (R) and products (P) are provided as the input vector x to the generator G. The filter sizes of each convolution are provided below the convolutional layers. G contains eight convolutions, while D contains three. Real pair (x, y) and fake pair (x, z) are concatenated into a tensor $\oplus$ (in green) that is provided to the discriminator, which predicts the probability of z being fake or real. Once the model is trained, synthetic TS (CM of TS) can directly be predicted from CMs of the reactant and product. The guess geometry of the TS is calculated from the corresponding CM.

and the loss l is defined by

$$l = \sum_{i=1}^{N}\sum_{i=j}^{N}\left(D_{ij}^{init} - D_{ij}^{ts}\right)^2. \tag{7}$$

Following the gradient of the loss l with respect to C, Eq. (5) is iterated until minimum l is reached. We utilized the default parameters from SciPy[74] *optimize.minimize* that uses the BFGS method for optimization. The number of steps depends on its default setting of convergence criteria of 1×10^{-5}. The TS guess coordinates for each atom are determined by reshaping the $(1 \times 3N)\mathbf{C}_{ts}$ vector to $(N \times 3)\mathbf{C}_{TS}$ vector, where each column is the coordinate for each atom,

$$\mathbf{C}_{TS} = \begin{Bmatrix} C_1 & C_2 & C_3 \\ . & . & \\ . & . & C_{3N} \end{Bmatrix}. \tag{8}$$

In order to validate the performance of the TS-GAN model, the root-mean-square deviation (RMSD) is used to measure the differences between real and predicted structures according to the following equation:

$$RMSD = \sqrt{\sum_{i=1}^{N}(\hat{y}_i - y_i)^2/N}, \tag{9}$$

where $\hat{y}_i$ and y_i are the predicted and actual values of the geometry of each atom i, respectively. $\hat{y}_i$ is determined by minimizing the *RMSD* by translating and rotating $\mathbf{C}_{TS}$ based on the Kabsch algorithm,[75] widely used in cheminformatics for aligning two chemical structures.

III. RESULTS AND DISCUSSION

A. TS-GAN model

The TS-GAN model is based on a deep generative framework as detailed by Isola *et al.*,[5] which takes input as the coordinates of the reactant and product to output the TS guess geometry. In the process, the reactant and product coordinates are first converted into constant size CMs and provided to the model to predict the CM of the TS guess geometry. The CM of TS guess is converted to coordinates of each atoms as detailed in Sec. II.

A GAN loss does not reach a minimum as it involves a zero sum game. The two neural networks generator and discriminator maximize one's action to minimize the other. The context of maximizing and minimizing implies the competition between the generator and discriminator as mentioned in Sec. II. The competition is articulated in such a manner that the generator has to minimize its objective while the discriminator has to maximize it. In this manner, both the generator and discriminator improve their respective performance of predicting the CM for the guess TS geometry that should have indistinguishable data distribution from the actual CM of the TS geometry. However, the GAN loss cannot be investigated on the progress of training TS-GAN due to no minimum. To analyze the training progress in a holistic way, we use the "real vs fake" tactic.[5] During the training process, a batch of random (real) samples of CM are selected from the dataset, and after each iteration, the model generates (fake) samples. Figure 2 shows the CMs for a random reactant and product pair at the end of the training progress. The CMs of the real and predicted TS guess geometry are visually similar. We monitored the RMSD deviation between the real and predicted CM for a random reactant and product pair over the progress of training to analyze the training progress. We observed that the RMSD deviation decreases over the number of iterations and reaches convergence, signifying that the model has been trained. The RMSD deviation

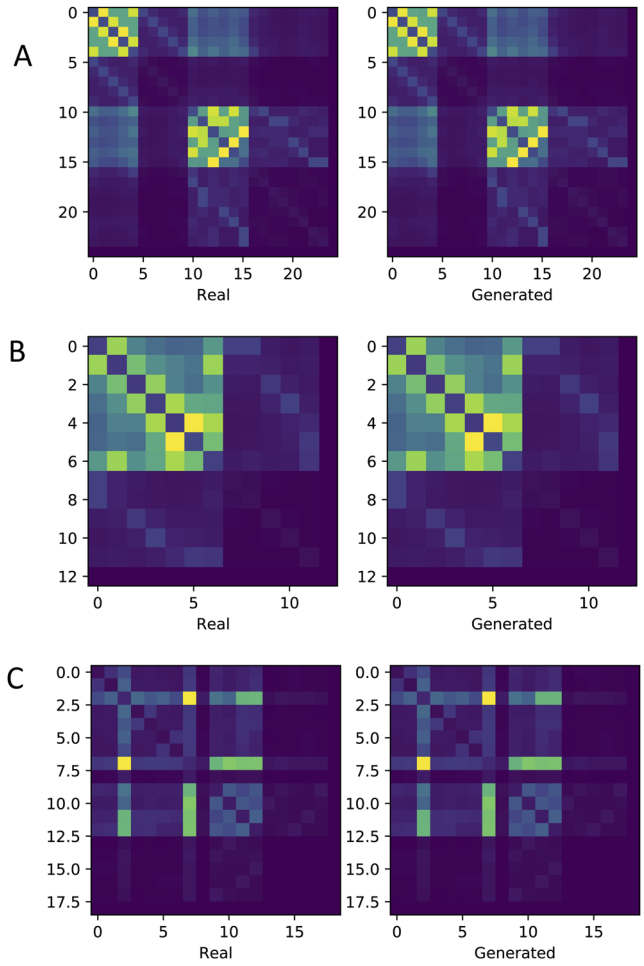

FIG. 2. An example of the real and generated Coulomb matrices randomly chosen from datasets **A**, **B**, and **C**, and shown as a heatmap.

over the number of iterations for the three datasets is shown in Fig. S1 of the supplementary material. The heatmaps and the RMSD deviations both show that the TS-GAN model was efficient in the training process predicting TS guess CMs very similar to real TS CMs.

B. TS guess geometry prediction

The predicted TS guesses from the TS-GAN model were analyzed based on the geometry. However, geometrical analysis can only be performed based on simple heuristics that can be directly compared. Dataset **A** features hydrogen migration and thus allows the possibility of checking the hydrogen distances between a hydrogen donor (D) and the corresponding acceptor (A). As shown in Fig. 3, we observe similar distributions for the mean of hydrogen (H) distances between H-D and H-A for the real and generated TS guesses. The majority of H-D/H-A distances are on an average 1.45 Å, which is a typical bond length of the H-bonds in hydrogen migration.[76]

The minimal movement of atoms in dataset **A** allows analyzing further chemical intuition from the predicted TS guess geometry.

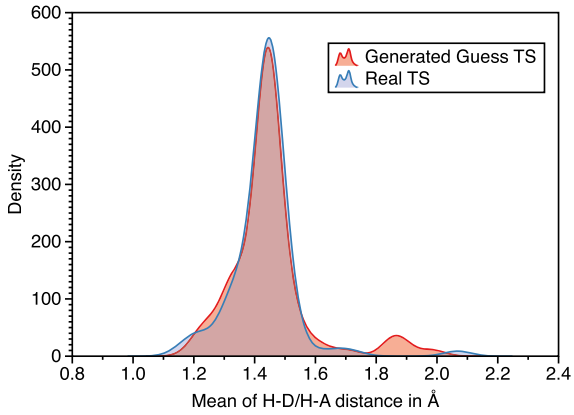

FIG. 3. Mean of the distances between donor-hydrogen and hydrogen-acceptor for all 120 reactions in the test set of dataset **A**.

As stated by Hammond[13] in 1955, a chemical reaction involving the reactant, product, and an intermediate TS will have the TS geometry closer to either the reactant or the product depending on the least energy difference. We sorted all chemical reactions to have reactants at higher energy than the product. Thus, all chemical reactions are made exothermic in nature, and therefore, the reactant and TS geometry should be more similar to the product and TS geometry. Figure 4(a) verifies the hypothesis where we observe that the RMSD between the reactant and TS geometry is smaller and, therefore, is more similar compared to the product and TS geometry. Similar results were observed for the generated TS guess geometries from the TS-GAN model as shown in Fig. 4(b). Note that Fig. 4(a) shows an extension toward the negative side of the plot due to the smoothening process (default settings of DataGraph[77]) of few reactions with RMSD between the reactant/product and TS being close to zero. However, the generated guess TS geometries do not have minute RMSD differences from the reactant/product, and therefore, the probability curve does not extend toward the negative region [Fig. 4(b)]. The generated guess TS geometries usually have larger RMSD compared to real TS geometries, due to the noise added from the GAN setting and minimization process to obtain coordinates from CM, which slightly changes the internal coordinates (bond length and angles and dihedrals). We further note that such an analysis cannot be made for dataset **B**, as the multiple atom movement leads to a random distribution of RMSD shown in Fig. S2.

C. TS-GAN applicability

Finding the correct TS depends on the space confined to reactants, products, and a good starting TS geometry. Figure 5 shows a typical energy profile of a three-step chemical reaction, where the TS(II) connecting intermediates R and products P is of interest. A guess TS geometry will only lead to the desired TS(II) if it has the correct orientation, reflected by the normal mode belonging to the imaginary frequency. The TS optimization is generally carried out following the normal mode associated with the imaginary frequency.[24] However, caused by the complexity of the PES, a slight change in the guess TS geometry can lead to a wrong TS; as depicted in Fig. 5, one may end up at TS(I) or TS(III) both connected with

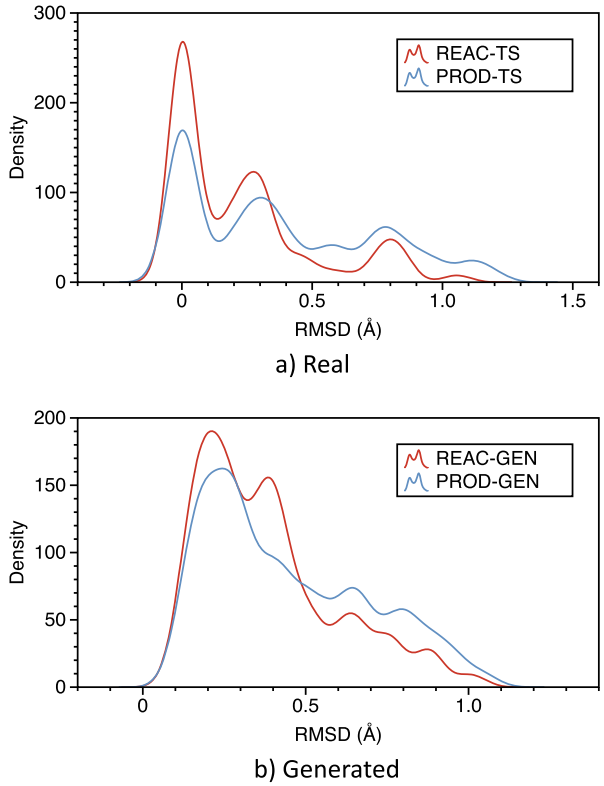

FIG. 4. The distribution of difference in RMSD values between the reactant and TS and the product and TS geometry for all 120 reactions in the test set of dataset **A** for (a) real and (b) generated TS. REAC, PROD, TS, and GEN refers to reactant, product, TS, and generated TS, respectively. All reactions are sorted to be exothermic and, therefore, we observe TS to be more similar to the reactant verifying the Hammond's postulate.

lower energy barriers. Thus, besides the geometry, the energy plays a dominant role.

We utilized two methods for optimizing the TS geometry for direct comparison with the TS-GAN model. The first method is Berny geometry optimization,[14] a classical approach following the smallest imaginary frequency from a guess geometry to the TS geometry. We start from the mean of reactant and product coordinates as the guess geometry to search for the TS geometry (here called the GTS method). The second method is the synchronous transit-guided quasi-Newton (QST2) method,[15] which requires the reactant and product geometry as the input. It is important to highlight that the QST2 method requires TS without intervening intermediates and, therefore, only a qualitative comparison between TS-GAN and QST2 methods can be performed and not quantitative. The two methods are widely applied in quantum chemistry to obtain the TS geometry. We note that the GTS method was used for the TS-GAN model to optimize the TS geometry from the predicted TS guess geometry. In all further references, TS-GAN refers to GTS optimized TS geometries based on predicted TS guess geometries unless stated otherwise. The TS optimization and Hessian calculations were done using the same DFT level as used for optimizing the test sets in Sec. II A. For each calculation, the Cartesian coordinates were used with Hessian computed at every cycle of optimization. The default values for the step size were implemented from Gaussian16 software that depends on the number of internal coordinates.[78]

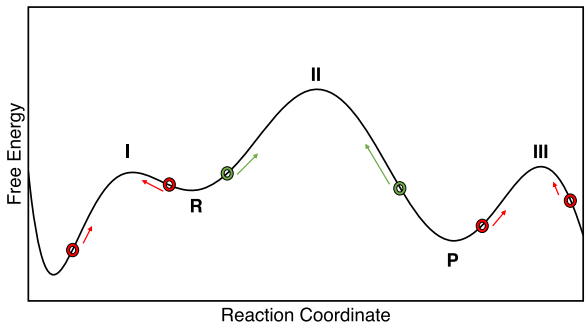

FIG. 5. Sketch of a free energy profile for a three-step chemical reaction. R and P are the intermediate reactant and product of interest. There are three TSs, denoted by I, II, and III, respectively, where TS(II) is the TS connecting R and P.

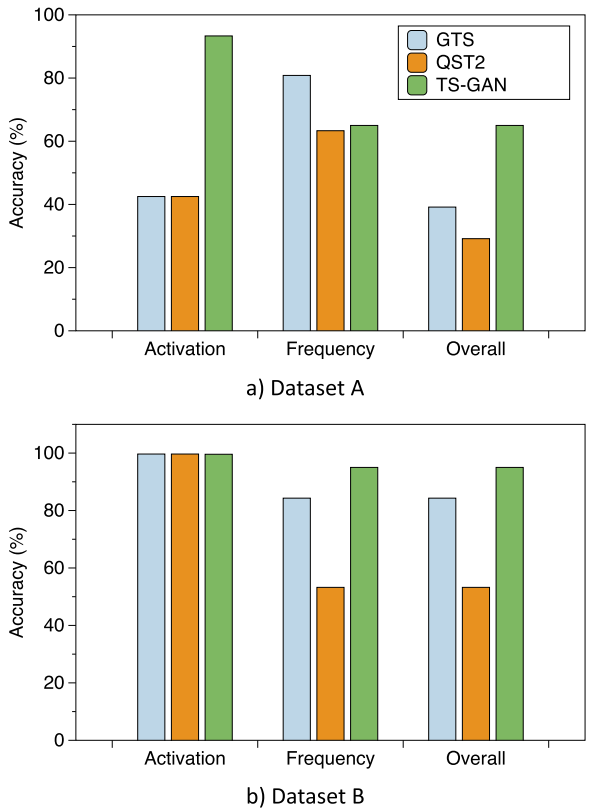

FIG. 6. Accuracy of TS geometry prediction based on the three methods: GTS, QST2, and TS-GAN for (a) 120 reactions in the test set of dataset **A** and (b) 1900 reactions in the test set of dataset **B**. Activation and frequency denote the accuracy in predicting the positive activation energy and one imaginary frequency, respectively. The overall accuracy considers activation, frequency, and the number of cycles for optimization, which should be less than 200 for correct prediction.

The TS geometry is first analyzed by quantifying that the activation energy is greater than zero. As denoted in Fig. 5, the TS energy should always be greater than both the reactant and product. Energies lower than either the reactant or product are basically not related to the real TS. The second analysis relates to the number of cycles required to reach convergence. The optimization process that took more than 200 cycles is labeled as the convergence error and, therefore, has the wrong TS guess geometry. The third analysis is based on the imaginary frequencies, which can be either none, one, or more than one. The TS geometry is labeled as correct when one and only one imaginary frequency is observed, denoting the saddle point. Any other scenario is labeled as a wrong TS guess geometry. Thus, the overall accuracy of a method is labeled as correct when all three criteria are satisfied.

Figure 6 shows the results obtained from the GTS, QST2, and TS-GAN methods. Dataset **A** is composed of hydrogen migrations. The starting structures for the QST2 method were the reactant and product corresponding to the intermediate (local energy minima's around the intermediate). The dataset is complex as multiple comparable hydrogen atoms have the possibility of migrating from one atom to the other. The GTS and QST2 methods show a low performance of 42% compared to TS-GAN (92%) in identifying the correct TS geometry based on the activation energy. GTS, QST2, and TS-GAN methods correctly identified one imaginary frequency for 81%, 64%, and 65%, respectively. However, multiple TS geometries with one imaginary frequency predicted by GTS and QST2 methods failed in identifying the correct geometry as observed by the activation energy, leading to poor performances of 39% and 29%,

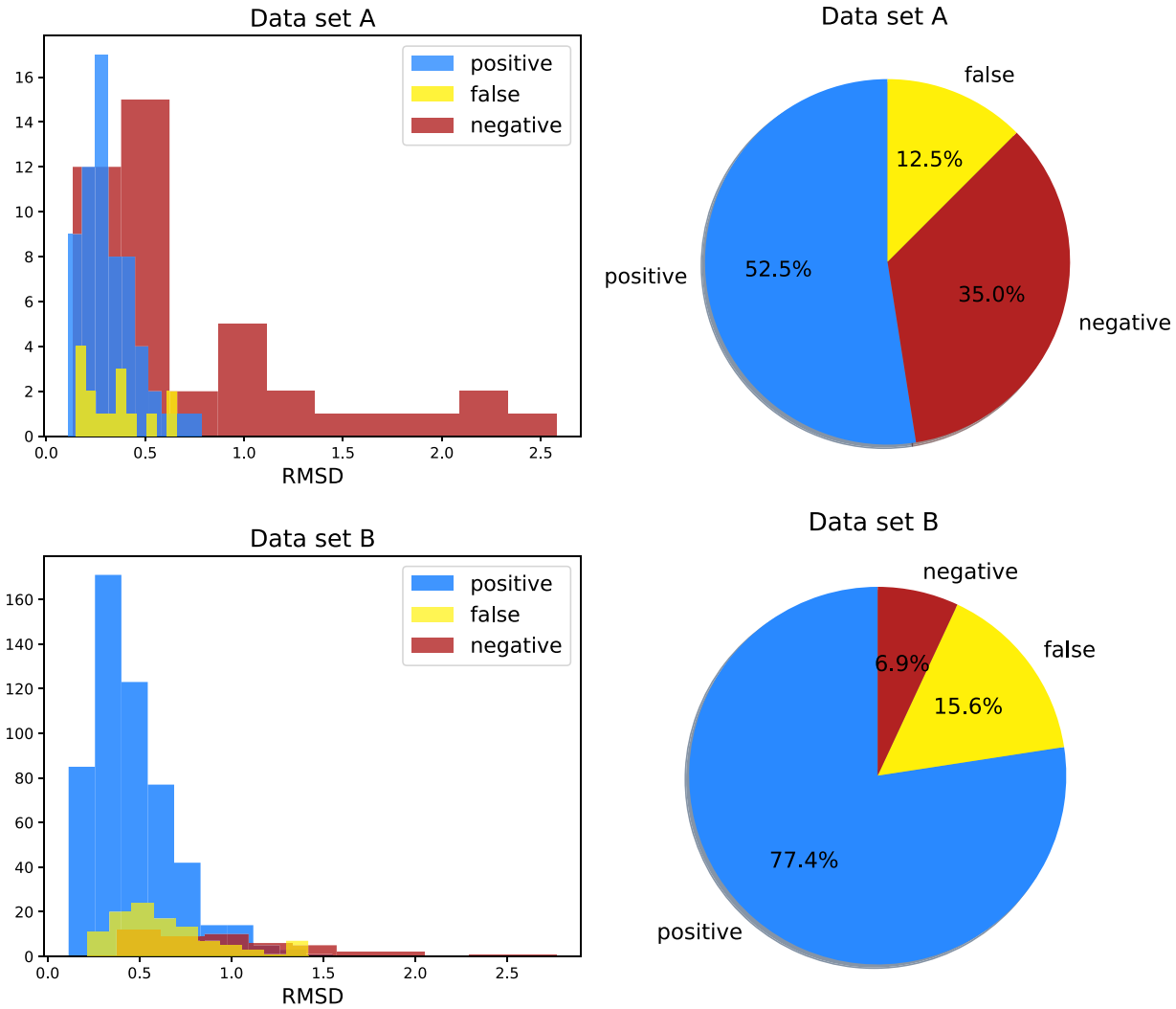

FIG. 7. The distribution of RMSD values for predicted TS guess geometries for positives, false negatives (false), and negatives are shown as a histogram. The success rate in identifying the correct TS geometries are shown as pie charts.

respectively. Dataset **B** is composed of isomerization reactions only and, therefore, involved multiple atoms movement for the reaction. The multi-dimensional PES for the isomerization reaction makes it complex to find the correct TS geometry as several saddle points exist for the compound. The activation energy is correctly predicted for all three methods, as shown in Fig. 6(b). However, the QST2 method fails for a significant portion (47%) of the isomerization reactions based on the imaginary frequency. The GTS and TS-GAN methods correctly predict one imaginary frequency for 84% and 95%, respectively. TS-GAN shows a remarkable performance with an overall accuracy of 95%.

Having made sure that the TS-GAN model is able to guess the correct TS geometry, we shift our focus toward the smallest frequency and its relation with the geometry. The optimized TS geometries from the TS-GAN model based on the TS guess geometry are labeled as positive, negative, and false. Positives are those complexes where the generated TS geometrically resembles the real structure, and the TS optimized correctly (i.e., imaginary frequency corresponds to the expected vibration). Negatives are those systems for which the TS optimization failed due to a wrong TS geometry leading to either no imaginary frequency or multiple imaginary frequency or convergence error within 200 cycles. False negatives are the generated structures that have more symmetry planes or different rotations of certain atoms in the molecule. Note that the false negative TS guess geometry optimized to the correct TS geometry. Examples for each of

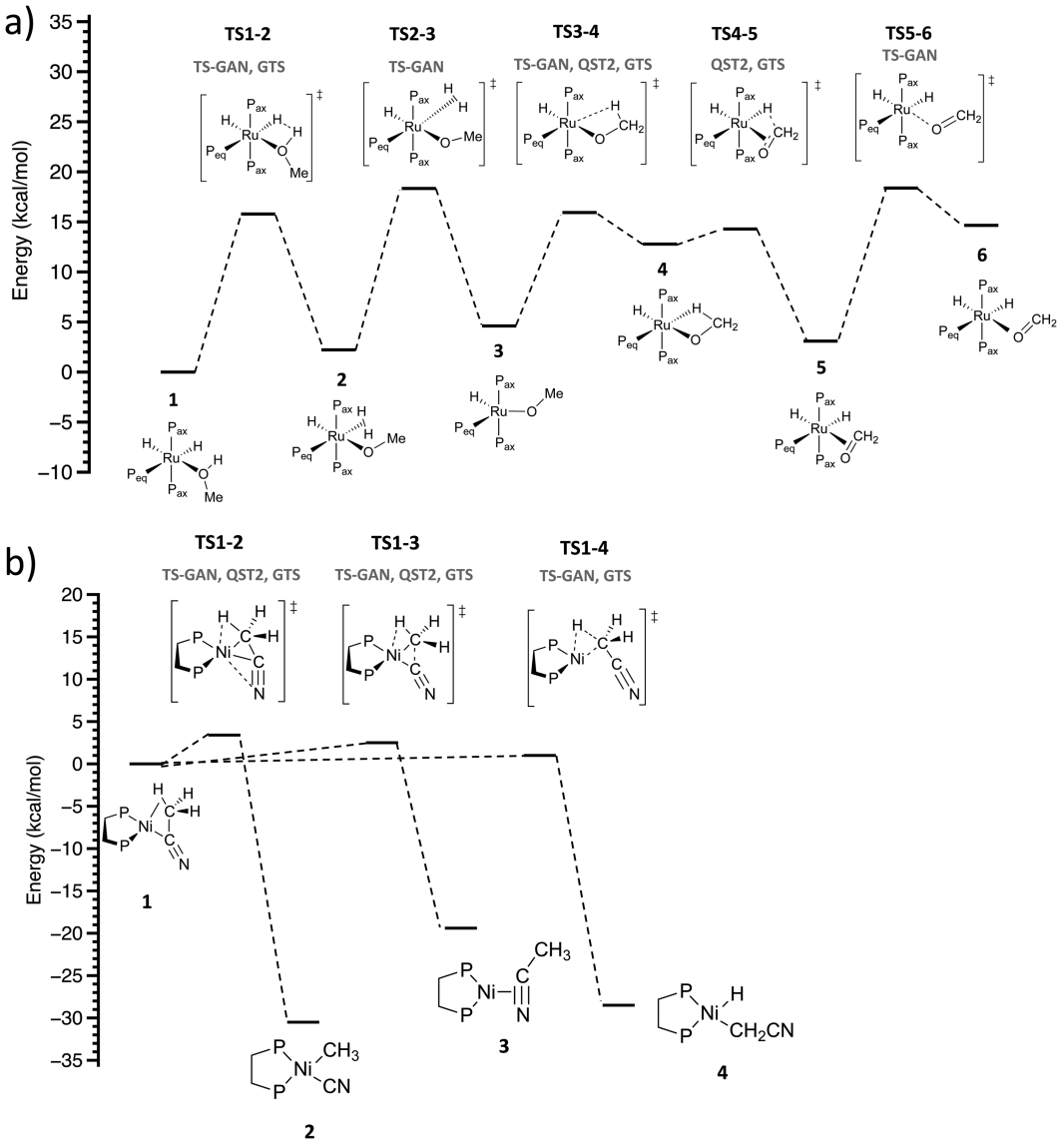

FIG. 8. Multi-step reaction for (a) ruthenium-trimethylphosphine catalyzed hydrogen transfer from alcohol and (b) nickel bis-dimethyl-phosphino-ethane [Ni(dmpe)] catalysts. Transition state structures were predicted based on the intermediates as starting points. In green color are marked structures predicted by TS-GAN, QST2, or GTS.

the labels, i.e., positive, negative and false negative, are shown in Fig. S2.

Figure 7 shows the RMSD distribution of the generated TS guess geometry and the corresponding pie chart with the annotated labels. The majority of the predicted TSs are positive and have RMSD values below 1.0 Å for both datasets **A** and **B** with an accuracy of 53% and 77%, respectively. The distribution of RMSD values is based on the noise in the CM of the TS guess geometry. This results in deviation of bond lengths, angles, and dihedrals for the atoms involved in the TS guess geometry. However, such slight changes do not interrupt the optimization process for the correct TS geometry. The negative labels have wide distribution of RMSD values ranging from 0.5 to 2.6 Å. Negative structures with relatively low RMSD values between 0.5 and 1.2 Å show that the generated TS guess geometry resembles the real TS; however, the TS optimization failed during converge, which in many cases include self-consistent field (SCF) optimization failures. The higher RMSD values for the negative labels correspond to failure in the distance matrix generated from the TS-GAN model. The false negative labels, similar to positives, have low RMSD values of less than 1.0 and 1.5 Å for datasets **A** and **B**, respectively.

The possibility of predicting multi-step reactions by TS-GAN is explored through dataset **C**, which contains 15 chemical reactions, with either Ni, Ru, or Au transition metal atoms. Similarly, as in the previous examples, we compared TS-GAN, QST2, and GTS methods. Figure 8 shows two reaction profiles of catalysts containing Ru and Ni, while the corresponding reaction of Ru and Au-catalysts is presented in Fig. S3. Transition states are predicted based on the intermediates. For example, **TS2-3** was predicted using intermediates **2** and **3** as starting structures. Additionally, Fig. 8 shows whether TS structures are predicted by TS-GAN, QST2, or GTS.

Figure 8(a) presents the energy profile of the ruthenium-trimethylphosphine catalyzed hydrogen transfer from alcohol. RMSD values range from 0.28 to 0.55 Å, showing that the generated TS guess is geometrically close to the real TS. The generated TS guess geometry from TS-GAN was able to successfully reach the correct TS geometry for four out of five intermediates in the reaction. The QST2 method correctly detected the TS geometry for two, while GTS detected for three out of the five intermediates. Additionally, we analyzed a similar reaction with Ru-bimethylphosphine. As shown in Fig. S3 of the supplementary material, the TS-GAN predicted all TS structures correctly for given intermediates.

We further looked at the reaction of the C–C and C–H bond activation of acetonitrile by a zerovalent nickel bis-dimethylphosphino-ethane [Ni(dmpe)] catalysts.[79] This multi-product reaction starts with an η3-H,C,C-acetonitrile complex containing an agostic C–H interaction with the metal center. As shown in Fig. 8(b), this stable species (**1**) lies on a relatively flat surface connecting to transition states leading to products **2**, **3**, and **4**. The RMSD values between the generated guess geometry and original TS are in the range 0.28–0.84 Å. TS-GAN and GTS predicted correctly all three TSs, while QST2 predicted only two.

The third multi-step reaction involves the hydroalkoxylation of allenes using N-heterocyclic carbene gold(I) complexes, [NHC]Au(I).[80] The reaction profile is presented in Fig. S3. The generated guess geometries are similar to the real TS, which is confirmed by RMSD values of 0.62 and 0.23 Å. TS-GAN predicts both TS structures, which lead to the correct TS geometry.

Cartesian coordinates of the generated TS structures are available in the supplementary material.

IV. CONCLUSIONS

We discuss in this work how a generative adversarial network can be applied to predict transition state guess geometries based on the Cartesian coordinates of reactants and products. The TS-GAN model was trained on three separate datasets, predicting transition state guesses for the H-migration reactions, isomerization reactions, and transition-metal catalyzed reactions. We showed that the TS-GAN model can be a powerful tool for predicting the TS guess geometry for reactions similar to those trained. For example, dataset **A** involves hydrogen migration reaction, and therefore, the trained model for this dataset can be used to predict TS guess geometries for all reactions that involve hydrogen migration. Similarly, the model trained on dataset **B** can be used to predict TS guess geometries for isomerization reactions, while transition metal-based reactions can be predicted on the model trained on dataset **C**.

A direct comparison with classical approaches proves the efficiency of our new TS-GAN method providing guess geometries that are close to the optimized ones. Additionally, we observed that the TS-GAN model follows Hammond's postulate and, therefore, is selective in generating TS guesses for a particular reaction with multiple intermediates and several energy pathways. In the case of dataset **C**, the TS-GAN model showed promise in generating good TS guesses for the multi-step reactions involved in the catalytic cycles of homogeneous transition metal catalysis.

In summary, we provide a new framework for finding TS guess geometries that can be easily applied and extended to any dataset that contains sufficient chemical reactions for training. The software is freely available for training, experimentation, and prediction at https://github.com/ekraka/TS-GAN.

SUPPLEMENTARY MATERIAL

The supplementary material contains citations to original papers related to the transition metal catalysis reactions contained in dataset **C**; RMSD between real and generated TS over the iteration number for datasets **A**, **B**, and **C**; RMSD distributions of dataset **B** for reactions in the test set; and energy profiles for Ru and Au catalysts.

AUTHORS' CONTRIBUTIONS

M.Z.M. and N.V. contributed equally to this work.

ACKNOWLEDGMENTS

This work was supported by the National Science Foundation, Grant No. CHE 1464906. The authors acknowledge SMU for providing generous computational resources.

DATA AVAILABILITY

The entire suite of TS-GAN scripts for training and predicting and all Coulomb matrices are provided through

https://github.com/ekraka/TS-GAN. Additional data are available in the supplementary material.

REFERENCES

[1]J. Gui, Z. Sun, Y. Wen, D. Tao, and J. Ye, "A review on generative adversarial networks: Algorithms, theory, and applications," arXiv:2001.06937 (2020).
[2]D. Saxena and J. Cao, "Generative adversarial networks (GANs): Challenges, solutions, and future directions," ACM Computing Surveys **54**, 1–42 (2021).
[3]Q. Vanhaelen, Y.-C. Lin, and A. Zhavoronkov, "The advent of generative chemistry," ACS Med. Chem. Lett. **11**, 1496–1505 (2020).
[4]I. Goodfellow, J. Pouget-Abadie, M. Mirza, B. Xu, D. Warde-Farley, S. Ozair, A. Courville, and Y. Bengio, "Generative adversarial networks," in *Neural Information Processing Systems* (Association for Computing Machinery (ACM), 2014), pp. 139–144.
[5]P. Isola, J.-Y. Zhu, T. Zhou, and A. A. Efros, "Image-to-image translation with conditional adversarial networks," arXiv:1611.07004 (2016).
[6]J. L. Bao and D. G. Truhlar, "Variational transition state theory: Theoretical framework and recent developments," Chem. Soc. Rev. **46**, 7548–7596 (2017).
[7]H. B. Schlegel, "Exploring potential energy surfaces for chemical reactions: An overview of some practical methods," J. Comput. Chem. **24**, 1514–1527 (2003).
[8]H. P. Hratchian and H. B. Schlegel, "Finding minima, transition states, and following reaction pathways on *ab initio* potential energy surfaces," in *Theory and Applications of Computational Chemistry* (Elsevier, 2005), pp. 195–249.
[9]J. M. Bofill, W. Quapp, and M. Caballero, "Locating transition states on potential energy surfaces by the gentlest ascent dynamics," Chem. Phys. Lett. **583**, 203–208 (2013).
[10]J. M. Bofill and J. M. Anglada, "Finding transition states using reduced potential-energy surfaces," Theor. Chem. Acc. **105**, 463–472 (2001).
[11]H. Guo and K. Liu, "Control of chemical reactivity by transition-state and beyond," Chem. Sci. **7**, 3992–4003 (2016).
[12]Z. Ren, Z. Sun, D. Zhang, and X. Yang, "A review of dynamical resonances in A + BC chemical reactions," Rep. Prog. Phys. **80**, 026401 (2016).
[13]G. S. Hammond, "A correlation of reaction rates," J. Am. Chem. Soc. **77**, 334–338 (1955).
[14]H. B. Schlegel, "Optimization of equilibrium geometries and transition structures," J. Comput. Chem. **3**, 214–218 (1982).
[15]C. Peng and H. B. Schlegel, "Combining synchronous transit and quasi-Newton methods to find transition states," Isr. J. Chem. **33**, 449–454 (1993).
[16]P. Y. Ayala and H. B. Schlegel, "A combined method for determining reaction paths, minima, and transition state geometries," J. Chem. Phys. **107**, 375–384 (1997).
[17]R. Lindh, A. Bernhardsson, G. Karlström, and P.-Å. Malmqvist, "On the use of a Hessian model function in molecular geometry optimizations," Chem. Phys. Lett. **241**, 423–428 (1995).
[18]M. J. D. Powell, "Recent advances in unconstrained optimization," Math. Program. **1**, 26–57 (1971).
[19]J. M. Bofill, "Updated Hessian matrix and the restricted step method for locating transition structures," J. Comput. Chem. **15**, 1–11 (1994).
[20]D. F. Shanno, "Conditioning of quasi-Newton methods for function minimization," Math. Comput. **24**, 647 (1970).
[21]R. Fletcher, *Practical Methods of Optimization* (John Wiley & Sons, Ltd., 2000).
[22]A. B. Birkholz and H. B. Schlegel, "Exploration of some refinements to geometry optimization methods," Theor. Chem. Acc. **135**, 84 (2016).
[23]A. Denzel and J. Kästner, "Hessian matrix update scheme for transition state search based on Gaussian process regression," J. Chem. Theory Comput. **16**, 5083–5089 (2020).
[24]H. B. Schlegel, "Geometry optimization," Wiley Interdiscip. Rev.: Comput. Mol. Sci. **1**, 790–809 (2011).
[25]P. M. Zimmerman, "Single-ended transition state finding with the growing string method," J. Comput. Chem. **36**, 601–611 (2015).
[26]P. L. Bhoorasingh and R. H. West, "Transition state geometry prediction using molecular group contributions," Phys. Chem. Chem. Phys. **17**, 32173–32182 (2015).
[27]C. W. Gao, J. W. Allen, W. H. Green, and R. H. West, "Reaction mechanism generator: Automatic construction of chemical kinetic mechanisms," Comput. Phys. Commun. **203**, 212–225 (2016).
[28]V. Ingman, A. Schaefer, L. Andreola, and S. Wheeler, "QChASM: Quantum chemistry automation and structure manipulation," Wiley Interdiscip. Rev.: Comput. Mol. Sci. **11**, e1510-1–e1510-12 (2020).
[29]B. J. Rooks, M. R. Haas, D. Sepúlveda, T. Lu, and S. E. Wheeler, "Prospects for the computational design of bipyridine *N*, *N*′-dioxide catalysts for asymmetric propargylation reactions," ACS Catal. **5**, 272–280 (2014).
[30]P. L. Bhoorasingh, B. L. Slakman, F. S. Khanshan, J. Y. Cain, and R. H. West, "Automated transition state theory calculations for high-throughput kinetics," J. Phys. Chem. A **121**, 6896–6904 (2017).
[31]L. D. Jacobson, A. D. Bochevarov, M. A. Watson, T. F. Hughes, D. Rinaldo, S. Ehrlich, T. B. Steinbrecher, S. Vaitheeswaran, D. M. Philipp, M. D. Halls, and R. A. Friesner, "Automated transition state search and its application to diverse types of organic reactions," J. Chem. Theory Comput. **13**, 5780–5797 (2017).
[32]W. M. C. Sameera, S. Maeda, and K. Morokuma, "Computational catalysis using the artificial force induced reaction method," Acc. Chem. Res. **49**, 763–773 (2016).
[33]S. Maeda, K. Ohno, and K. Morokuma, "Systematic exploration of the mechanism of chemical reactions: The global reaction route mapping (GRRM) strategy using the ADDF and AFIR methods," Phys. Chem. Chem. Phys. **15**, 3683 (2013).
[34]S. Maeda and K. Morokuma, "Toward predicting full catalytic cycle using automatic reaction path search method: A case study on $HCo(CO)_3$-catalyzed hydroformylation," J. Chem. Theory Comput. **8**, 380–385 (2012).
[35]M. Gao, A. Lyalin, S. Maeda, and T. Taketsugu, "Application of automated reaction path search methods to a systematic search of single-bond activation pathways catalyzed by small metal clusters: A case study on H–H activation by gold," J. Chem. Theory Comput. **10**, 1623–1630 (2014).
[36]E. Martínez-Núñez, "An automated transition state search using classical trajectories initialized at multiple minima," Phys. Chem. Chem. Phys. **17**, 14912–14921 (2015).
[37]A. W. Senior, R. Evans, J. Jumper, J. Kirkpatrick, L. Sifre, T. Green, C. Qin, A. Žídek, A. W. R. Nelson, A. Bridgland, H. Penedones, S. Petersen, K. Simonyan, S. Crossan, P. Kohli, D. T. Jones, D. Silver, K. Kavukcuoglu, and D. Hassabis, "Improved protein structure prediction using potentials from deep learning," Nature **577**, 706–710 (2020).
[38]J. E. Hein, "Machine learning made easy for optimizing chemical reactions," Nature **590**, 40–41 (2021).
[39]B. Sanchez-Lengeling, J. N. Wei, B. K. Lee, R. C. Gerkin, A. Aspuru-Guzik, and A. B. Wiltschko, "Machine learning for scent: Learning generalizable perceptual representations of small molecules," arXiv:1910.10685 (2019).
[40]N. Verma, X. Qu, F. Trozzi, M. Elsaied, N. Karki, Y. Tao, B. Zoltowski, E. C. Larson, and E. Kraka, "SSnet: A deep learning approach for protein-ligand interaction prediction," Int. J. Mol. Sci. **22**, 1392 (2021).
[41]R. Srinivas, N. Verma, E. Kraka, and E. C. Larson, "Deep learning-based ligand design using shared latent implicit fingerprints from collaborative filtering," J. Chem. Inform. Model **61**, 2159–2174 (2021).
[42]S. Manzhos and T. Carrington, Jr., "Neural network potential energy surfaces for small molecules and reactions," Chem. Rev. (published online).
[43]O. T. Unke, D. Koner, S. Patra, S. Käser, and M. Meuwly, "High-dimensional potential energy surfaces for molecular simulations: From empiricism to machine learning," Mach. Learn.: Sci. Technol. **1**, 013001-1–013001-22 (2020).
[44]P. O. Dral, "Quantum chemistry in the age of machine learning," J. Phys. Chem. Lett. **11**, 2336–2347 (2020).
[45]O. V. Prezhdo, "Advancing physical chemistry with machine learning," J. Phys. Chem. Lett. **11**, 9656–9658 (2020).
[46]*Machine Learning Meets Quantum Physics*, edited by K. T. Schütt, S. Chmiela, O. A. von Lilienfeld, A. Tkatchenko, K. Tsuda, and K.-R. Müller (Springer International Publishing, 2020).
[47]A. Denzel, B. Haasdonk, and J. Kästner, "Gaussian process regression for minimum energy path optimization and transition state search," J. Phys. Chem. A **123**, 9600–9611 (2019).
[48]I. F. Galván, G. Raggi, and R. Lindh, "Restricted-variance constrained, reaction path, and transition state molecular optimizations using gradient-enhanced kriging," J. Chem. Theory Comput. **17**, 571–582 (2020).

[49]K. Jorner, T. Brinck, P.-O. Norrby, and D. Buttar, "Machine learning meets mechanistic modelling for accurate prediction of experimental activation energies," Chem. Sci. **12**, 1163–1175 (2021).
[50]Z. D. Pozun, K. Hansen, D. Sheppard, M. Rupp, K.-R. Müller, and G. Henkelman, "Optimizing transition states via kernel-based machine learning," J. Chem. Phys. **136**, 174101 (2012).
[51]L. Pattanaik, J. B. Ingraham, C. A. Grambow, and W. H. Green, "Generating transition states of isomerization reactions with deep learning," Phys. Chem. Chem. Phys. **22**, 23618–23626 (2020).
[52]L. Goerigk, A. Hansen, C. Bauer, S. Ehrlich, A. Najibi, and S. Grimme, "A look at the density functional theory zoo with the advanced GMTKN55 database for general main group thermochemistry, kinetics and noncovalent interactions," Phys. Chem. Chem. Phys. **19**, 32184–32215 (2017).
[53]J. Baker and F. Chan, "The location of transition states: A comparison of Cartesian, Z-matrix, and natural internal coordinates," J. Comput. Chem. **17**, 888–904 (1996).
[54]A. D. Becke, "Density-functional exchange-energy approximation with correct asymptotic behavior," Phys. Rev. A **38**, 3098–3100 (1988).
[55]C. Lee, W. Yang, and R. G. Parr, "Development of the Colle-Salvetti correlation-energy formula into a functional of the electron density," Phys. Rev. B **37**, 785–789 (1988).
[56]B. P. Pritchard, D. Altarawy, B. Didier, T. D. Gibson, and T. L. Windus, "New basis set exchange: An open, up-to-date resource for the molecular sciences community," J. Chem. Inf. Model. **59**, 4814–4820 (2019).
[57]Y.-S. Lin, G.-D. Li, S.-P. Mao, and J.-D. Chai, "Long-range corrected hybrid density functionals with improved dispersion corrections," J. Chem. Theory Comput. **9**, 263–272 (2012).
[58]K. Fukui, "The path of chemical reactions—The IRC approach," Acc. Chem. Res. **14**, 363–368 (1981).
[59]C. A. Grambow, L. Pattanaik, and W. H. Green, "Reactants, products, and transition states of elementary chemical reactions based on quantum chemistry," Sci. Data **7**, 137 (2020).
[60]E. Kraka, W. Zou, Y. Tao, and M. Freindorf, "Exploring the mechanism of catalysis with the unified reaction valley approach (URVA)—A review," Catalysts **10**, 691 (2020).
[61]M. Rupp, A. Tkatchenko, K.-R. Müller, and O. A. von Lilienfeld, "Fast and accurate modeling of molecular atomization energies with machine learning," Phys. Rev. Lett. **108**, 058301 (2012).
[62]K. Hansen, G. Montavon, F. Biegler, S. Fazli, M. Rupp, M. Scheffler, O. A. von Lilienfeld, A. Tkatchenko, and K.-R. Müller, "Assessment and validation of machine learning methods for predicting molecular atomization energies," J. Chem. Theory Comput. **9**, 3404–3419 (2013).
[63]F. Häse, S. Valleau, E. Pyzer-Knapp, and A. Aspuru-Guzik, "Machine learning exciton dynamics," Chem. Sci. **7**, 5139–5147 (2016).
[64]O. Çaylak, A. Yaman, and B. Baumeier, "Evolutionary approach to constructing a deep feedforward neural network for prediction of electronic coupling elements in molecular materials," J. Chem. Theory Comput. **15**, 1777–1784 (2019).
[65]C.-I. Wang, I. Joanito, C.-F. Lan, and C.-P. Hsu, "Artificial neural networks for predicting charge transfer coupling," J. Chem. Phys. **153**, 214113 (2020).
[66]M. Krämer, P. M. Dohmen, W. Xie, D. Holub, A. S. Christensen, and M. Elstner, "Charge and exciton transfer simulations using machine-learned Hamiltonians," J. Chem. Theory Comput. **16**, 4061–4070 (2020).
[67]M. Rinderle, W. Kaiser, A. Mattoni, and A. Gagliardi, "Machine-learned charge transfer integrals for multiscale simulations in organic thin films," J. Phys. Chem. C **124**, 17733–17743 (2020).
[68]D. C. Elton, Z. Boukouvalas, M. S. Butrico, M. D. Fuge, and P. W. Chung, "Applying machine learning techniques to predict the properties of energetic materials," Sci. Rep. **8**, 9059 (2018).
[69]X. Li and J. Saude, "Explain graph neural networks to understand weighted graph features in node classification," arXiv:2002.00514 (2020).
[70]Coulomb matrices of the datasets presented in this paper are available as npy files in the folder test-cases, https://github.com/ekraka/TS-GAN, 2021.
[71]D. Pathak, P. Krahenbuhl, J. Donahue, T. Darrell, and A. A. Efros, "Context encoders: Feature learning by inpainting," in *2016 IEEE Conference on Computer Vision and Pattern Recognition (CVPR)* (IEEE, 2016), pp. 2536–2544; arXiv:1604.07379.
[72]R. Zhang, P. Isola, and A. A. Efros, "Colorful image colorization," in *European Conference on Computer Vision (ECCV)* (Springer International Publishing, 2016), pp. 649–666.
[73]R. Fu, B. Li, Y. Gao, and P. Wang, "Visualizing and analyzing convolution neural networks with gradient information," Neurocomputing **293**, 12–17 (2018).
[74]P. Virtanen, R. Gommers, T. E. Oliphant, M. Haberland, T. Reddy, D. Cournapeau, E. Burovski, P. Peterson, W. Weckesser, J. Bright, S. J. van der Walt, M. Brett, J. Wilson, K. J. Millman, N. Mayorov, A. R. J. Nelson, E. Jones, R. Kern, E. Larson, C. J. Carey, İ. Polat, Y. Feng, E. W. Moore, J. VanderPlas, D. Laxalde, J. Perktold, R. Cimrman, I. Henriksen, E. A. Quintero, C. R. Harris, A. M. Archibald, A. H. Ribeiro, F. Pedregosa, P. van Mulbregt, and SciPy 1.0 Contributors, "SciPy 1.0: Fundamental algorithms for scientific computing in Python," Nat. Methods **17**, 261–272 (2020).
[75]W. Kabsch, "A solution for the best rotation to relate two sets of vectors," Acta Crystallogr., Sect. A **32**, 922–923 (1976).
[76]J. J. Dannenberg, "An Introduction to Hydrogen Bonding by George A. Jeffrey (University of Pittsburgh). Oxford University Press: New York and Oxford. 1997," J. Am. Chem. Soc. **120**, 5604 (1998).
[77]DataGraph, Version 4.6, Visual DataTools, Inc. Chapel Hill, NC, https://www.visualdatatools.com/, 2020.
[78]M. J. Frisch, G. W. Trucks, H. B. Schlegel, G. E. Scuseria, M. A. Robb, J. R. Cheeseman, G. Scalmani, V. Barone, G. A. Petersson, H. Nakatsuji, X. Li, M. Caricato, A. V. Marenich, J. Bloino, B. G. Janesko, R. Gomperts, B. Mennucci, H. P. Hratchian, J. V. Ortiz, A. F. Izmaylov, J. L. Sonnenberg, D. Williams-Young, F. Ding, F. Lipparini, F. Egidi, J. Goings, B. Peng, A. Petrone, T. Henderson, D. Ranasinghe, V. G. Zakrzewski, J. Gao, N. Rega, G. Zheng, W. Liang, M. Hada, M. Ehara, K. Toyota, R. Fukuda, J. Hasegawa, M. Ishida, T. Nakajima, Y. Honda, O. Kitao, H. Nakai, T. Vreven, K. Throssell, J. A. Montgomery, Jr., J. E. Peralta, F. Ogliaro, M. J. Bearpark, J. J. Heyd, E. N. Brothers, K. N. Kudin, V. N. Staroverov, T. A. Keith, R. Kobayashi, J. Normand, K. Raghavachari, A. P. Rendell, J. C. Burant, S. S. Iyengar, J. Tomasi, M. Cossi, J. M. Millam, M. Klene, C. Adamo, R. Cammi, J. W. Ochterski, R. L. Martin, K. Morokuma, O. Farkas, J. B. Foresman, and D. J. Fox, Gaussian 16, Revision C.01, Gaussian, Inc., Wallingford, CT, 2016.
[79]T. A. Ateşin, T. Li, S. Lachaize, W. W. Brennessel, J. J. García, and W. D. Jones, "Experimental and theoretical examination of C–CN and C–H bond activations of acetonitrile using zerovalent nickel," J. Am. Chem. Soc. **129**, 7562–7569 (2007).
[80]M. Z. Makoś, M. Freindorf, Y. Tao, and E. Kraka, "Theoretical insights into [NHC]Au(I) catalyzed hydroalkoxylation of allenes: A unified reaction valley approach study," J. Org. Chem. **86**, 5714–5726 (2021).